ARTICLE OPEN

Check for updates

The PIP4K2 inhibitor THZ-P1-2 exhibits antileukemia activity by disruption of mitochondrial homeostasis and autophagy

Keli Lima[1,2], Diego Antonio Pereira-Martins[1,3], Lívia Bassani Lins de Miranda[2], Juan Luiz Coelho-Silva[4], Giovana da Silva Leandro[5], Isabel Weinhäuser[1,3], Rita de Cássia Cavaglieri[1], Aline de Medeiros Leal[1], Wellington Fernandes da Silva[1], Ana Paula Alencar de Lima Lange[1], Elvira Deolinda Rodrigues Pereira Velloso[1], Emmanuel Griessinger[3], Jacobien R. Hilberink[3], Emanuele Ammatuna[3], Gerwin Huls[3], Jan Jacob Schuringa[3], Eduardo Magalhães Rego[1]✉ and João Agostinho Machado-Neto[2]✉

The treatment of acute leukemia is challenging because of the genetic heterogeneity between and within patients. Leukemic stem cells (LSCs) are relatively drug-resistant and frequently relapse. Their plasticity and capacity to adapt to extracellular stress, in which mitochondrial metabolism and autophagy play important roles, further complicates treatment. Genetic models of phosphatidylinositol-5-phosphate 4-kinase type 2 protein (PIP4K2s) inhibition have demonstrated the relevance of these enzymes in mitochondrial homeostasis and autophagic flux. Here, we uncovered the cellular and molecular effects of THZ-P1-2, a pan-inhibitor of PIP4K2s, in acute leukemia cells. THZ-P1-2 reduced cell viability and induced DNA damage, apoptosis, loss of mitochondrial membrane potential, and the accumulation of acidic vesicular organelles. Protein expression analysis revealed that THZ-P1-2 impaired autophagic flux. In addition, THZ-P1-2 induced cell differentiation and showed synergistic effects with venetoclax. In primary leukemia cells, LC-MS/MS-based proteome analysis revealed that sensitivity to THZ-P1-2 is associated with mitochondrial metabolism, cell cycle, cell-of-origin (hematopoietic stem cell and myeloid progenitor), and the TP53 pathway. The minimal effects of THZ-P1-2 observed in healthy $CD34^+$ cells suggest a favorable therapeutic window. Our study provides insights into the pharmacological inhibition of PIP4K2s targeting mitochondrial homeostasis and autophagy, shedding light on a new class of drugs for acute leukemia.

Blood Cancer Journal (2022)12:151 ; https://doi.org/10.1038/s41408-022-00747-w

INTRODUCTION

Acute leukemia comprises a heterogeneous group of highly aggressive hematological malignancies. In adults, both acute myeloid leukemia (AML) and acute lymphoblastic leukemia (ALL) have high rates of relapse and poor prognoses [1, 2]. Significant advances have been made in understanding the molecular basis of these diseases, which has allowed the identification of diagnostic markers, prognostic factors, and novel FDA-approved targeted therapies [3–5]. However, their therapeutic repertoire remains limited. Recent studies have indicated a prominent role for mitochondrial metabolism in the therapeutic response of these neoplasms, revealing the increased sensitivity of leukemic stem cells (LSC) to disruptions of oxidative phosphorylation (OXPHOS) [6, 7]. These vulnerabilities may be specifically targeted by the BCL2 inhibitor venetoclax, which suppresses the tricarboxylic acid (TCA) cycle by inhibiting amino acid metabolism [8–10]. Additionally, autophagy and lysosomal biosynthesis have emerged as potential targets for improving therapeutic responses to these diseases [11, 12].

The phosphatidylinositol-5-phosphate 4-kinase type 2 (PIP4K2s) family comprises three lipid kinase members (PIP4K2A, PIP4K2B, and PIP4K2C), which phosphorylate phosphatidylinositol (PI)5 P at position four of the inositol ring, generating PI-4,5-P_2 [13]. Furthermore, these enzymes have been associated with the local and specialized generation of PI-4,5-P2 pools in intracellular membranes, which are critical for the functionality of endosomes, autophagosomes, lysosomes, and peroxisomes [14–17].

Under physiological conditions, PI-4,5-P_2-mediated signaling is implicated in many cellular processes, including proliferation, survival, glucose uptake, and cytoskeletal organization, which have been reported to be deregulated in breast cancer, acute leukemias, glioblastoma, and soft tissue sarcomas [13, 18]. Cancer genomic and transcriptomic landscape studies have revealed that PIP4K2-related genes are usually not mutated, but their expression is frequently altered [13]. In ALL, single nucleotide polymorphisms (SNPs) in the regulatory regions of the *PIP4K2A* gene are associated with increased mRNA levels and risk of disease development [19, 20]. In hematological malignancies, PIP4K2A has been identified as an essential protein for the proliferation, clonogenicity, and survival of leukemia-initiating cells [21]. In AML patients, high *PIP4K2A* and *PIP4K2C* transcript levels are associated

[1]Laboratory of Medical Investigation in Pathogenesis and Targeted Therapy in Onco-Immuno-Hematology (LIM-31), Department of Internal Medicine, Hematology Division, Faculdade de Medicina, University of São Paulo, São Paulo, Brazil. [2]Department of Pharmacology, Institute of Biomedical Sciences, University of São Paulo, São Paulo, Brazil. [3]Department of Experimental Hematology, Cancer Research Center Groningen, University Medical Center Groningen, University of Groningen, Groningen, Netherlands. [4]Department of Medical Imaging, Hematology, and Oncology, Ribeirão Preto Medical School, University of São Paulo, Ribeirão Preto, Brazil. [5]Department of Microbiology, Institute of Biomedical Sciences, University of São Paulo, São Paulo, Brazil. ✉email: eduardo.rego@fm.usp.br; jamachadoneto@usp.br

Received: 31 August 2022 Revised: 17 October 2022 Accepted: 20 October 2022
Published online: 09 November 2022

with adverse cytogenetic risks and poor clinical outcomes [22, 23]. THZ-P1-2 is a prototype for a new class of drugs that acts as a selective pan-inhibitor of PIP4K2s. This drug covalently binds to a single cysteine residue located in a disordered loop close to the ATP-binding site of the kinase domain in the three PIP4K2 isoforms, which irreversibly inhibits the activity of these enzymes. Genetic inhibition of PIP4K2s indicates that inhibition of at least two isoforms (PIP4K2A/B) is necessary to obtain a pronounced biological effect [16, 24, 25], suggesting that selective pharmacological inhibitors for more than one isoform are of interest. Initial studies have shown that THZ-P1-2 reduces cell viability by inhibiting autophagic flux in solid tumors [26], but its efficacy in acute leukemia has not yet been explored. Here, we show that THZ-P1-2 has potent antileukemic effects in AML and ALL and uncover the underlying molecular mechanisms.

MATERIAL AND METHODS

Patients

Bone marrow or peripheral blood samples from patients with AML and ALL were used after obtaining informed consent, and the protocol was approved by the Ethical Committee of the Institute of Biomedical Sciences of the University of São Paulo (CAAE:39510920.1.0000.5467) or the Medical Ethical Committee of the UMCG in accordance with the Declaration of Helsinki. Mononuclear cells were isolated by density gradient separation (Ficoll, Sigma-Aldrich, St. Louis, MO, USA) according to the manufacturer's instructions. An overview of the patient characteristics is described in Supplementary Tables 1–3. Neonatal cord blood (CB) samples were obtained from healthy full-term pregnancies in accordance with the Declaration of Helsinki at the obstetrics departments of the Martini Hospital University Medical Center Groningen. $CD34^+$ cells were isolated using an autoMACS hematopoietic progenitor magnetic-associated cell-sorting kit (#130-046-703, Miltenyi Biotech, Bergisch Gladbach, Germany) according to the manufacturer's instructions.

Cell lines and inhibitors

OCI-AML3, Kasumi-1, MOLM-13, and MV4-11 cells were obtained from Deutsche Sammlung von Mikroorganismen and Zellkulturen (DSMZ, Germany). THP-1 and HL-60 cells were obtained from American Type Culture Collection (ATCC, USA). NB4 cells were kindly provided by Prof. Pier Paolo Pandolfi (Beth Israel Deaconess Medical Center, Havard Medical School, Boston, USA). U-937, K-562, KU812, HEL, Jurkat, Namalwa, Daudi, and Raji cells were kindly provided by Prof. Sara Teresinha Olalla Saad (University of Campinas, Campinas, Brazil). CEM, NALM6, and REH were kindly provided by Gilberto Carlos Franchi Junior (University of Campinas, Campinas, Brazil). SET-2 cells were kindly provided by Prof. Fabíola Attié de Castro (University of São Paulo, Ribeirão Preto, Brazil). SUP-B15 was provided by Dr. Lucas Eduardo Botelho de Souza (National Institute of Science and Technology in Stem Cells and Cell Therapy, Ribeirão Preto, Brazil). MOLT-4 cells were kindly provided by Prof. Gisele Monteiro (University of São Paulo, São Paulo, Brazil). Cells were cultured in appropriate media (RPMI-1640, IMDM, or alpha-MEM) supplemented with 10 or 20% fetal bovine serum (FBS) according to the ATCC and DSMZ recommendations, plus 1% penicillin/streptomycin, and maintained at 5% CO_2 and 37 °C. THZ-P1-2 was obtained from MedChemExpress (Monmouth Junction, NJ, USA) and diluted to 25 mM in dimethyl sulfoxide (Me_2SO_4; DMSO). Venetoclax (ABT-199) was obtained from TargetMol (Target Molecule Corp. Boston, MA, USA) and diluted to a 50 mM stock solution in DMSO. Cytarabine (AraC) was obtained from Accord (Accord Healthcare B.V. Utrecht, Netherlands) and diluted to 1 mM stock solution in DMSO.

Cell viability assay

In total, 2×10^4 cells per well were seeded in a 96-well plate in the appropriate medium in the presence of vehicle or different concentrations of THZ-P1-2 (1.6, 3.2, 6.4, 12.5, 25, 50, or 100 µM) for 24, 48, or 72 h. Next, 10 µl methylthiazoletetrazolium (MTT, Sigma-Aldrich) solution (5 mg/mL) was added and incubated at 37 °C, 5% CO_2 for 4 h. The reaction was stopped using 100 µL of 0.1 N HCl in anhydrous isopropanol. Cell viability was evaluated by measuring absorbance at 570 nm. IC_{50} values were calculated by nonlinear regression analysis using GraphPad Prism 5 (GraphPad Software, Inc. San Diego, CA, USA).

Cell cycle assay

In total, 6×10^5 cells per well were seeded in 6-well plates supplemented with vehicle or THZ-P1-2 (1.6, 3.2, and 6.4 µM), harvested at 24 h, fixed with 70% ethanol, and stored at 4 °C for at least 2 h. Next, the Fixed cells were stained with 20 µg/mL propidium iodide (PI) containing 10 µg/mL RNase A for 30 min at room temperature in a light-protected area. The DNA content distribution was determined using flow cytometry (FACSCalibur; Becton Dickinson, FranklinLakes, NJ, USA) and analyzed using FlowJo software (Treestar, Inc. San Carlos, CA, USA).

Comet assay

For the alkaline comet assay, MV4-11 and Jurkat cells (1.5×10^5 per 35 mm cell culture dish) were treated with vehicle or THZ-P1-2 (3.2 and 6.4 µM) for 48 h. Next, cells were counted and suspended at a concentration of 1×10^5 cells/mL. A total of 12 µL of cell solution was suspended in low melting point (0.5%) agarose suspension in phosphate-buffered saline (PBS) at 37 °C, and solutions were added onto pre-coated CometAssay® Kit slides (Trevigen, Gaithersburg, MD, USA). After solidification of agarose, the slides were immersed in a cold lysis solution (Comet Assay Lysis Solution, Trevigen) for at least 40 min and protected from light. Under light protection, the slides were immersed in an alkaline solution (300 mM NaOH and 1 mM EDTA, pH 13.0) for 20 min to allow the unfolding of the DNA structure. Then, the slides were arranged horizontally in an electrophoresis vat with an alkaline solution (30 mM NaOH and 1 mM EDTA, pH 13.0) at 4 °C. Electrophoresis was performed at 300 mA and 4 °C for 30 min. After electroplating, the slides were neutralized with dH_2O for 5 min and fixed with 70% ethanol. For DNA staining, SYBR™ Green I nucleic acid gel stain (Invitrogen Molecular Probes, Eugene, OR, USA) was used for 5 min. The slides were analyzed under a Zeiss fluorescence microscope (Axiovert 200, Zeiss, Jena, Germany) with a 510–560 nm filter and a 590 nm barrier. The DNA head-to-tail ratio was scored from 100 comets on each slide and analyzed using the LUCIA Comet Assay™ software (Laboratory Image Prague, Czech Republic).

Apoptosis assay

In total, 1×10^5 cells per well were seeded in a 24-well plate in an FBS-supplemented medium in the presence of vehicle or THZ-P1-2 (1.6, 3.2, and 6.4 µM) for 24 h. Next, the cells were washed with ice-cold phosphate-buffered saline (PBS) and resuspended in a binding buffer containing 1 µg/mL propidium iodide (PI) and 1 µg/mL APC-labeled annexin V (BD Pharmingen, San Diego, CA, USA). All specimens were analyzed using flow cytometry (FACSCalibur) after incubation for 15 min at room temperature in a light-protected area. Ten thousand events were recorded for each sample.

Mitochondrial membrane potential evaluation

In total, 1×10^5 cells per well were seeded in a 24-well plate in FBS-supplemented appropriate media in the presence of vehicle or THZ-P1-2 (1.6, 3.2, and 6.4 µM) for 24 h. Cells were then washed with PBS and resuspended in a buffer containing 5 µg/mL JC-1 (BD) and 10,000 events were acquired by flow cytometry (FACSCalibur) after incubation for 15 min at 37 °C and 5% CO_2 in a light-protected area. Alternatively, cells were stained with 100 nM tetramethylrhodamine, ethyl ester, and perchlorate (TMRE) according to the manufacturer's instructions (Thermo Fisher Scientific, Waltham, MA, USA), and 10,000 events were acquired by flow cytometry using BD LSR™II (BD Biosciences). The events were analyzed using the FlowJo software (Treestar, Inc.).

Acidic vesicular organelles staining by acridine orange

In total, 1×10^5 cells per well were seeded in a 24-well plate in FBS-supplemented appropriate media in the presence of vehicle or THZ-P1-2 (1.6, 3.2, and 6.4 µM) for 24 h. The cells were then washed with PBS and resuspended in PBS containing 0.1 µg/mL acridine orange (Sigma-Aldrich) and 10,000 events were acquired by flow cytometry (FACSCalibur) after incubation for 30 min at room temperature in a light-protected area and one wash with PBS. The events were analyzed using the FlowJo software (Treestar, Inc.). The recommendations published by Thomé et al. [27] were followed during data acquisition and analysis to avoid false positive results. Alternatively, OCI-AML3 and NALM6 cells stained with PBS containing 0.1 µg/mL acridine orange were evaluated for GFP and RFP channels using a fluorescent microscope (Lionheart FX Automated microscope; Agilent BioTek Instruments Inc., Santa Clara, CA, USA; magnification, ×400).

Western blotting

Cells were treated with vehicle or THZ-P1-2 (1.6, 3.2, or 6.4 μM) for 24 h and submitted to total protein extraction using a buffer containing 100 mM Tris (pH 7.6), 1% Triton X-100, 2 mM PMSF, 10 mM Na_3VO_4, 100 mM NaF, 10 mM $Na_4P_2O_7$, and 4 mM EDTA. Equal amounts of protein (30 μg) from the samples were subsequently subjected to SDS-PAGE in an electrophoresis device, followed by electrotransfer of the proteins to nitrocellulose membranes. The membranes were blocked with 5% non-fat dry milk and incubated with specific primary antibodies diluted in blocking buffer, followed by secondary antibodies conjugated to horseradish peroxidase (HRP). Western blot analysis was performed using a SuperSignal™ West Dura Extended Duration substrate system (Thermo Fisher Scientific) and G:BOX Chemi XX6 gel document system (Syngene Cambridge, UK). Antibodies directed against PARP1 (#9542), γH2AX (#9718), SQSTM1/p62 (#88588), LC3B (#2775), and α-tubulin (#2144) were obtained from Cell Signaling Technology (Danvers, MA, USA). Band intensities were determined using UN-SCAN-IT gel 6.1 software (Silk Scientific; Orem, UT, USA).

Quantitative RT-PCR (qRT-PCR)

Cells were treated with vehicle or THZ-P1-2 (6.4 μM) for 24 h, after which total RNA was extracted using the TRIzol reagent (Thermo Fisher Scientific). cDNA was synthesized from 1 μg RNA using a High-Capacity cDNA Reverse Transcription Kit (Thermo Fisher Scientific). Quantitative PCR (qPCR) was performed using a QuantStudio 3 Real-Time PCR System in conjunction with a SybrGreen System (Thermo Fisher Scientific) to assess the expression of cell cycle-, apoptosis-, and autophagy-related genes (Supplementary Table 4). *HPRT1* and *ACTB* were used as reference genes. Relative quantification values were calculated using the $2^{-\Delta\Delta CT}$ equation [28]. A negative "No Template Control" was included for each primer pair. Data were illustrated using Morpheus (https://software.broadinstitute.org/morpheus/).

Ex vivo assays

For cell viability evaluation by MTT assay, 2×10^5 mononuclear primary cells per well were seeded in a 96-well plate in the appropriate medium (AML samples: 30% FBS RPMI, 10 ng/mL IL3, 10 ng/mL FLT3L, 100 ng/mL TPO, 100 ng/mL SCF; ALL samples: 30% FBS RPMI, 30 ng/mL IL3, 100 ng/mL IL7, 100 ng/mL FLT3L, and 30 ng/mL SCF) in the presence of vehicle or different concentrations of THZ-P1-2 (1.6, 3.2, 6.4, 12.5, 25, 50, or 100 μM) for 72 h and analyzed as described above. All cytokines and growth factors were acquired from PeproTech (Rocky Hill, NJ, USA). The IC_{50} values were calculated by nonlinear regression analysis using GraphPad Prism 5.

Apoptosis and mitochondrial membrane potential analyses were performed using FITC-labeled annexin V/DAPI and TMRE staining, respectively, and flow cytometry analysis was performed in gated human $Sca1^-$ (to exclude MS5 contamination), $CD45^+$, $CD34^+$ (or $CD117^+$ for *NPM1*-mutant AMLs) cells. Briefly, mouse bone marrow-derived MS5-stromal cells were initially plated on gelatin-coated 24-well plates and expanded to form a confluent layer to which primary AML mononuclear cells were added. Primary AML cells were cultured in 12.5% FBS and 12.5% horse serum IMDM (Thermo Fisher Scientific), 1% penicillin and streptomycin (Life Technologies, Grand Island, NY, USA), and 57.2 μM β-mercaptoethanol (Merck Sharp & Dohme BV, Haarlem, Netherlands), with the addition of 20 ng/mL G-CSF (Amgen), N-Plate (clinical grade TPO) (Amgen), and IL3 (Sandoz). Cells were exposed to the vehicle, AraC (250 and 500 nM), venetoclax (100 and 500 nM), and/or THZ-P1-2 (3.2 and 6.4 μM) for 72 h. AraC and venetoclax were used as controls (AML-related cytotoxic drugs).

For growth curves, CB $CD34^+$ cells were expanded in the co-culture system with MS5-stromal cells in the presence of vehicle and THZ-P1-2 (3.2 and 6.4 μM). For colony formation assays, 300 CB $CD34^+$ cells were seeded on methylcellulose (H4230, Stem Cell Technologies, Vancouver, Canada) supplemented with SCF, FLT3L, N-plate (all 100 ng/mL), EPO, IL3, and IL-6 (all 20 ng/mL) in the presence of vehicle or THZ-P1-2 (3.2 and 6.4 μM). After 8 days for CFU-E/BFU-E and 14 days for CFU-G/GM, the colonies were identified and counted. All cell cultures were grown at 37 °C and 5% CO_2.

Proteome and gene set enrichment analysis (GSEA)

Proteomic analyses were performed as previously described (available at PRIDE under PXD030463) [29]. Gene set enrichment analysis (GSEA) was performed with GSEA v.4.0 [30] using the MSigDB curated gene sets Hallmarks, Reactome, and Kegg. Enrichment scores (ES) were calculated based on the Kolmogorov-Smirnov statistic, tested for significance using 1000 permutations, and normalized (NES) to take into account the size of each gene set. A significance cutoff of FDR q values < 0.25 was used.

Oxygen consumption and extracellular acidification rate measurements

Oxygen consumption rate (OCR) and extracellular acidification rate (ECAR) were measured using a Seahorse XF96 analyzer (Seahorse Bioscience Agilent, US) at 37 °C. A total of 1×10^5 cells (treated with vehicle or 6.4 μM THZ-P1-2 for 24 h) were seeded per well in poly-L-lysine (Sigma-Aldrich)-coated Seahorse XF96 plates in 200 μL XF Assay Medium (Modified DMEM, Seahorse Bioscience). For the OCR measurements, the XF assay medium was supplemented with 10 mM glucose. Oligomycin A (2.5 μM), FCCP (carbonyl cyanide-4-(trifluoromeththoxy) phenylhydrazone) (2.5 μM), and 2 μM antimycin (2 μM) plus rotenone (2 μM) were sequentially injected in 25 μL volume to measure basal and maximal OCR levels (all reagents from Sigma-Aldrich). For ECAR measurements, glucose-free XF assay medium was added to the cells, and 10 mM glucose, 2.5 μM oligomycin A, and 100 mM 2-deoxy-D-glucose were sequentially injected in a 25 μL volume (all reagents from Sigma-Aldrich). All XF96 protocols consisted of four mixes (2 min) and measurement (2 min) cycles, allowing for the determination of OCR at basal and between injections. Both basal and maximal OCR levels were calculated by assessing the metabolic response of the cells following the manufacturer's recommendations. OCR measurements were normalized to the number of viable cells used in the assay.

Cell differentiation analysis

OCI-AML3, THP-1, and NB4 cells were exposed to vehicle or THZ-P1-2 (1.6, 3.2, or 6.4 μM) for 72 h. Next, the cells were washed with ice-cold phosphate-buffered saline (PBS), resuspended in 100 μL PBS containing 5 μL of PE-labeled anti-CD11b (clone MEM-174, EXBIO Praha, Vestec, Czech Republic) or 5 μL of APC-labeled anti-CD14 (clone TÜK4), and incubated at room temperature in a light-protected area for 30 min. The cells were then washed with ice-cold PBS and resuspended in 300 μL of PBS. All specimens were obtained using flow cytometry (FACSCalibur) and analyzed using FlowJo software (Treestar, Inc.). For morphology analysis, cells (1×10^5) were adhered to microscopic slides using cytospin (Serocito, model 2400; FANEM Guarulhos, Brazil), followed by Rosenfeld staining. The morphologies of the nucleus and cytoplasm of the treated cells were observed under a Leica DM2500 optical microscope, and images were acquired using LAS software version 4.6 (Leica Bensheim, Germany).

Statistical analysis

Statistical analyses were performed using GraphPad Prism 8 (GraphPad Software, Inc.). ANOVA, Bonferroni post-test, and Student's t-test were used for comparisons as appropriate. Correlograms were constructed using the Morpheus software. All p values were two-sided with a significance level of 5%.

RESULTS

THZ-P1-2 reduces cell viability and induces DNA damage in leukemia cells

We investigated the role of PIP4K2s in the malignant phenotypes of AML and ALL using the candidate drug THZ-P1-2. Using a panel of 21 commonly used human myeloid and lymphoid leukemic cell lines, THZ-P1-2 caused a dose-dependent decrease in viability in these leukemia cells, with IC_{50} ranging from 5.6 to >100 μM for myeloid cells and 2.3 to 13.4 μM for lymphoid cells (Fig. 1A). The reduction in cell viability induced by THZ-P1-2 was time-dependent in leukemic cells (Fig. 1B). To gain a better understanding of the cellular mechanisms underlying the decrease in cell viability, we evaluated the DNA content of leukemia cells treated with vehicle or THZ-P1-2.

Our results indicated that cytostatic effects were associated with a reduction of cells in the S and G_2/M phases when THZ-P1-2 was administered at low concentrations (1.6 or 3.2 μM). Conversely, when THZ-P1-2 was administered at high concentrations (6.4 μM), we observed cytotoxic effects linked with an increased accumulation of cells in the $subG_1$ (all $p < 0.05$, Fig. 1C). The presence of DNA damage after exposure to THZ-P1-2 in leukemia cells was confirmed by the comet assay (all $p < 0.05$; Fig. 1D).

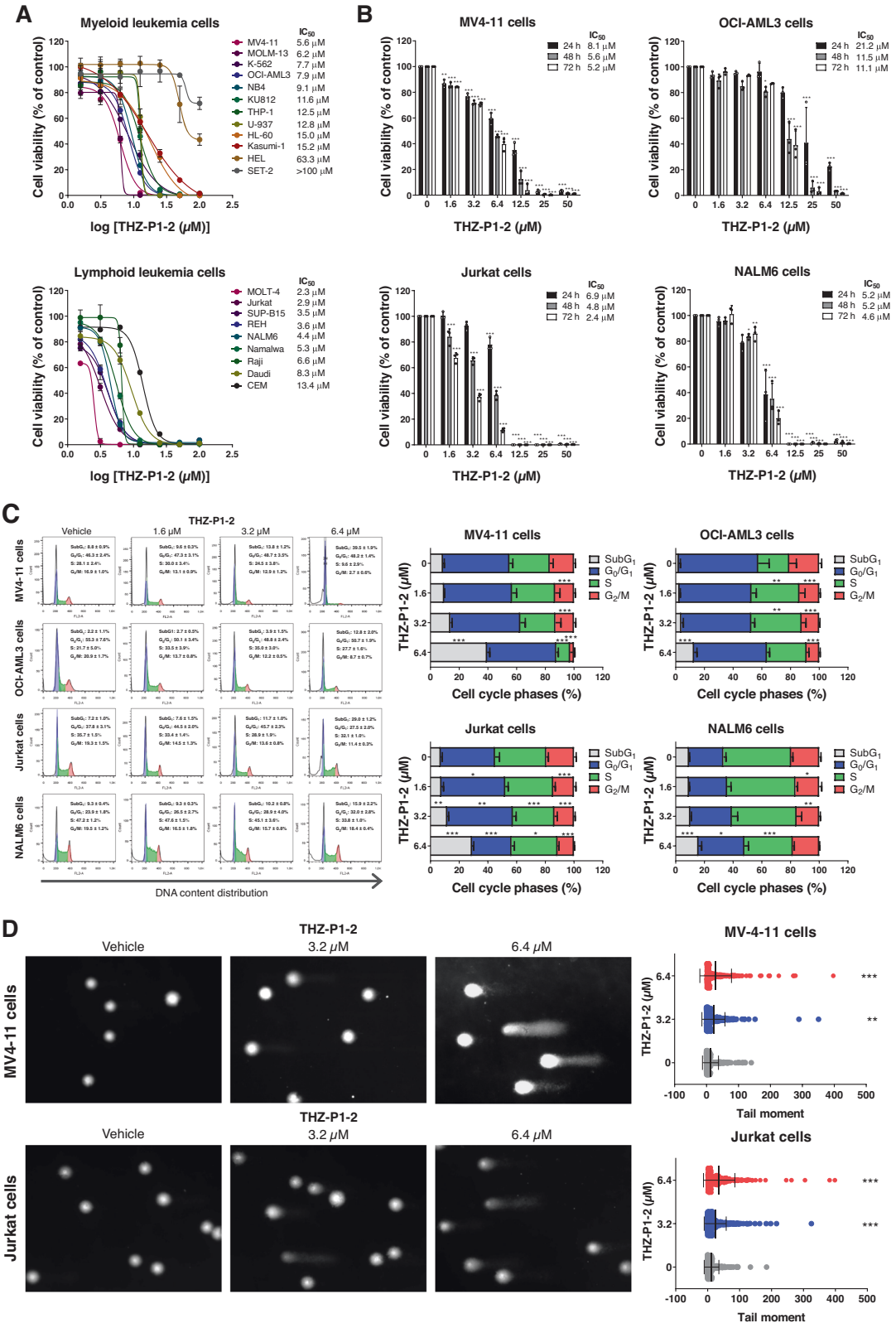

THZ-P1-2 triggers apoptosis and disrupts mitochondrial homeostasis and autophagic flux

Next, we evaluated the apoptotic effects of THZ-P1-2 on leukemic cells. An increase in apoptosis was detected in all cellular models upon treatment with THZ-P1-2, with the highest apoptotic rate observed in MV4-11 and Jurkat cells. (Fig. 2A). In line with our apoptosis data, we also observed a significant loss of mitochondrial membrane potential (MMP), indicating mitochondrial damage (Fig. 2B). However, the loss of MMP was not directly correlated with the frequency of apoptotic cells, especially in OCI-

Fig. 1 Pharmacological PIP4K2s inhibition reduces cell viability and induces DNA damage in leukemia cells. A Dose-response cytotoxicity was analyzed using a methylthiazoletetrazolium (MTT) assay in a panel of myeloid and lymphoid leukemic cell lines treated with vehicle or increasing concentrations of THZ-P1-2 (1.6, 3.2, 6.4, 12.5, 25, 50, and 100 μM) for 72 h. Values are expressed as the percentage of viable cells for each condition relative to vehicle-treated cells. The IC_{50} values and leukemia cell lines used are described in the figure. **B** Dose- and time-response cytotoxicity was evaluated by methylthiazoletetrazolium (MTT) in MV4-11, OCI-AML3, Jurkat, and NALM6 cells treated with vehicle or with increasing concentrations of THZ-P1-2 (1.6, 3.2, 6.4, 12.5, 25, and 50 μM) for 24, 48, and 72 h. Bar graphs represent values expressed as a percentage for each condition relative to vehicle-treated controls. Results are presented as the mean ± SD of at least three independent experiments. The *p* values and cell lines are indicated in the graphs; $*p < 0.05$; $**p < 0.01$; $***$ $p < 0.001$, ANOVA and Bonferroni post-test. **C** Phases of the cell cycle were determined by analyzing the DNA content by staining with propidium iodide and acquiring the data by flow cytometry following exposure of MV4-11, OCI-AML3, Jurkat, and NALM6 cells to the vehicle or THZ-P1-2 (1.6, 3.2, and 6.4 μM) for 24 h. A representative histogram for each condition is illustrated. The mean ± SD of at least three independent experiments is represented in the bar graph. The *p* values and cell lines are indicated in the graphs; $*p < 0.05$; $**p < 0.01$; $***p < 0.001$, ANOVA and Bonferroni post-test. **D** DNA damage was evaluated by the single-cell comet assay in MV4-11 and Jurkat treated with vehicle or THZ-P1-2 (3.2 or 6.4 μM) for 48 h. Scatter plots represent the tail moment values (head/tail DNA ratio) obtained using the LUCIA Comet Assay™ software. $**p < 0.01$; $***p < 0.001$, ANOVA and Bonferroni post-test.

AML3 and NALM6 cells, suggesting activation of resistance/survival pathways.

Previous studies using a murine genetic model deficient in *Pip4k2a*$^{-/-}$ and *Pip4k2b*$^{-/-}$ have shown that PIP4K2s are essential for the formation of autophagosomes [16]. Considering that autophagy has been linked to leukemogenesis and the recycling of damaged mitochondria [31], we evaluated the formation of acidic vesicular organelles (AVO) as a mechanism of resistance. Notably, AVO levels were substantially elevated upon THZ-P1-2 exposure, particularly at concentrations that induced lower levels of apoptosis (Fig. 2C, D), suggesting an inverse correlation between apoptosis and autophagy. At the molecular level, THZ-P1-2 induced the expression of apoptosis markers (PARP1 cleavage) and DNA damage (γH2AX) at levels comparable to those observed in the previous cellular assays. Furthermore, LC3BII and SQSTM1/p62 levels increased, indicating a failure to complete autophagic flow (Fig. 3A).

Exploratory analysis of genes associated with cell cycle progression, apoptosis, and autophagy revealed that seven genes were increased in all leukemic models analyzed (*CDKN1B*, *MCL1*, *BAX*, *BCL2L11*, *BBC3*, *MAP1LC3B*, and *ATG5*, all $p < 0.05$, Fig. 3B and Supplementary Table 5). These genes were significantly associated with the intrinsic apoptotic signaling pathway, signal transduction in the absence of ligands, autophagosome organization, macroautophagy, and response to starvation (all FDR $q < 0.05$), corroborating previous cellular and molecular findings (Fig. 3C).

THZ-P1-2 negatively impacts cellular metabolism in leukemia cells

Since the response to THZ-P1-2 was associated with mitochondrial damage and starvation in leukemic cells, we studied the effect of THZ-P1-2 on cellular metabolism. Our results confirmed that THZ-P1-2 exposure reduced the mitochondrial membrane potential of leukemia cells (Fig. 4A). In addition, exposure to THZ-P1-2 reduced basal and maximal cellular respiration capacity (Fig. 4B-D) as well as glycolytic flux (Fig. 4E, F), indicating that the drug negatively affects the metabolic state of leukemic cells.

THZ-P1-2 selectively reduces cell viability of primary leukemic blasts

To validate the antineoplastic potential of THZ-P1-2 in preclinical models of acute leukemias, primary cells from a heterogeneous set of patients diagnosed with de novo AML and ALL were subjected to ex vivo drug screening. Similar to what was observed in the cell line model, THZ-P1-2 reduced the viability of primary leukemic cells in a dose-dependent manner with IC_{50} ranging from 6.4 to >100 μM for AML samples and 3.1 to 31.2 μM for ALL samples (Fig. 5A). Furthermore, using a co-culture system, similar results were observed in an independent and functionally well-characterized AML cohort (Fig. 5B). Surprisingly, the response to THZ-P1-2 correlated with a more metabolically active phenotype (oxygen consumption and extracellular acidification) of leukemic blasts (Fig. 5C). Among the genetic markers related to AML, the presence of mutations in *FLT3*, *NPM1*, *RUNX1*, *IDH1*/2, and *DNMT3A* was not associated with drug response (Fig. 5D). *PIP4K2A*, *PIP4K2B*, and *PIP4K2C* mRNA levels were not associated with THZ-P1-2 response in ex vivo assays (all $p > 0.05$; Supplementary Table 6). In the context of healthy hematopoiesis, THZ-P1-2 only slightly reduced the proliferation of CB $CD34^+$ cells in long-term culture, while no difference in colony formation capacity was observed (Fig. 5E, F).

Mitochondrial dysfunction caused by THZ-P1-2 was also validated in primary leukemia cells (Fig. 5G, H). Proteome analysis was performed on samples from patients considered sensitive or resistant to THZ-P1-2, which presented distinct protein signatures (Fig. 5I). Gene enrichment analysis identified multiple processes and signaling pathways associated with mitochondrial metabolism, cell cycle stage, leukemic cell-of-origin, and the TP53 pathway (all FDR *q* value < 0.05, Fig. 5J, K). Taken together, these results suggest that patients with AML sensitive to THZ-P1-2 differ in their metabolic and proliferative states compared to resistant AMLs.

DISCUSSION

Here, we report the antileukemic effects of a novel PIP4K2 inhibitor, THZ-P1-2. In a targeted knockdown screen for phosphoinositide modulator-related genes, *PIP4K2A* was identified as essential for the survival, proliferation, and clonogenicity of leukemia-initiating cells in humans and murine models [21]. High transcript levels of *PIP4K2A* and *PIP4K2C* are predictive of poor prognosis in patients with AML [22, 23]. Furthermore, SNPs in the regulatory region of *PIP4K2A* are associated with increased mRNA levels and susceptibility to ALL development [19, 20]. These studies revealed a potential role for this family of enzymes in the malignant phenotype of human leukemia, which can serve as targets for treatment. Indeed, initial observations indicate that THZ-P1-2 reduces cell viability in six human leukemia cell lines, which was confirmed by us using a larger heterogeneous panel of leukemia cell lines and primary cells from two independent acute leukemia cohorts; however, the mechanisms involved remain poorly explored to date [26].

In this study, THZ-P1-2 reduced cell viability by disrupting mitochondrial homeostasis, cellular metabolism, and autophagy. The role of PIP4K2s in the regulation of energy metabolism and autophagy has been previously reported; in particular, the product of these enzymes, PI-4,5-P_2, has been described as necessary for the fusion of lysosomes with autophagosomes and to complete autophagic flux [16, 18, 26]. Considering our data, THZ-P1-2 was able to accurately phenocopy many of the cellular and molecular findings observed in PIP4K2s genetic inhibition models, including accumulation of SQSTM1/p62 and LC3BII [16]. There is also

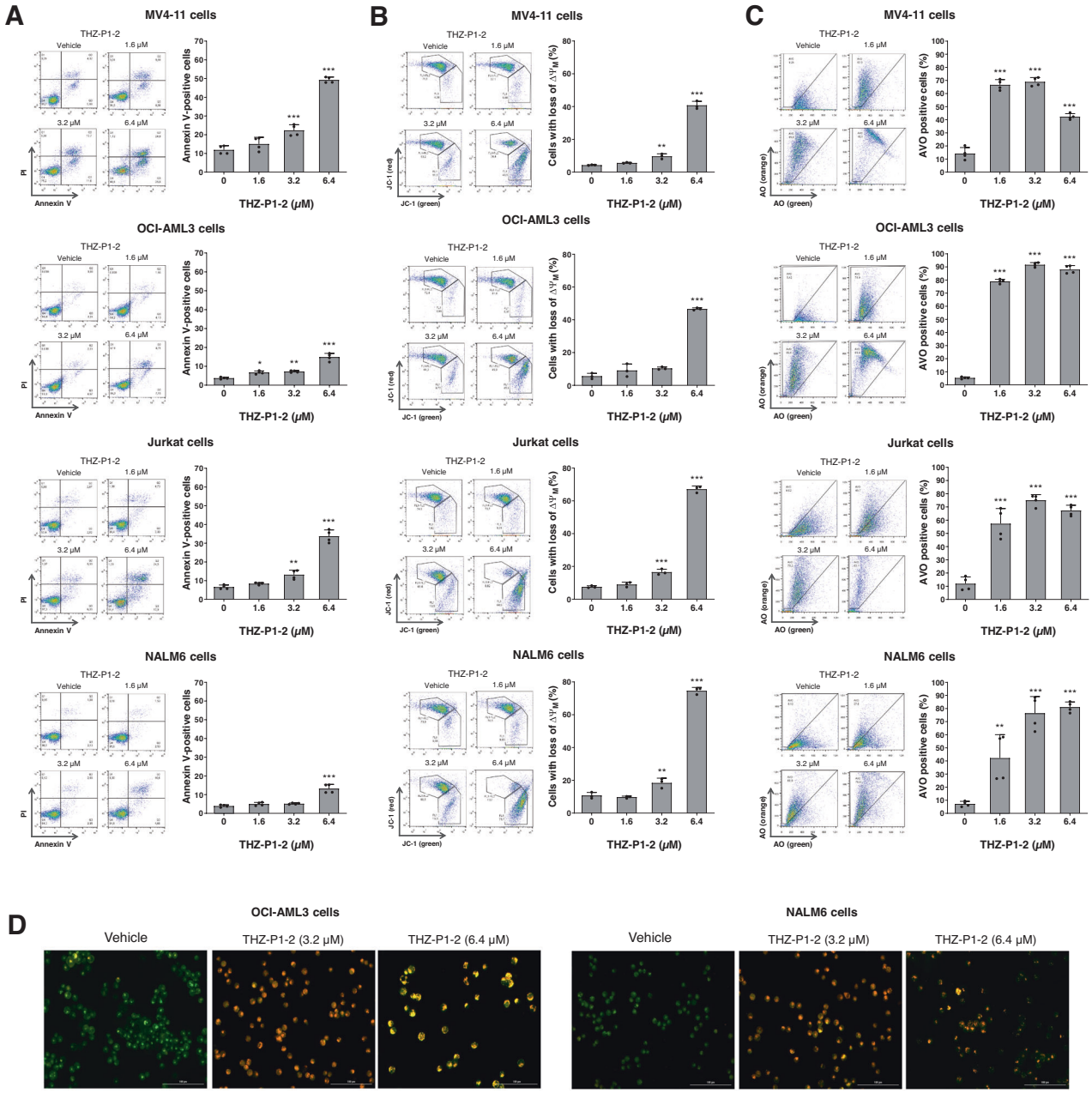

Fig. 2 THZ-P1-2 induces apoptosis and dysfunction in mitochondria and autophagic flux. A Apoptosis was detected by flow cytometry in MV4-11, OCI-AML3, Jurkat, and NALM6 cells treated with vehicle or with increasing concentrations of THZ-P1-2 (1.6, 3.2, and 6.4 μM) for 24 h using an APC-annexin V/PI staining method. Representative dot plots are shown for each condition. The upper and lower right quadrants (Q2 plus Q3) cumulatively contain the apoptotic cell population (annexin V^+ cells). Bar graphs represent the mean ± SD of at least three independent experiments. The *p* values and cell lines are indicated in the graphs; **p* < 0.05, ***p* < 0.01, ****p* < 0.0001; ANOVA and Bonferroni post-test. **B** Mitochondrial membrane potential ($\Delta\Psi_M$) analysis was evaluated using the JC-1 staining method and flow cytometry. Leukemic cells were treated with vehicle or THZ-P1-2 (1.6, 3.2, and 6.4 μM) for 24 h. Representative dot plots are shown for each condition; the gate FL-2 contains cells with intact mitochondria and the gate FL-2/FL-1 contains cells with damaged mitochondria. Bar graphs represent the mean ± SD of at least three independent experiments and the *p* values are indicated; ***p* < 0.01, ****p* < 0.0001; ANOVA and Bonferroni post-test. **C** The evaluation of acidic vesicular organelles (AVOs) was investigated through acridine orange (AO) labeling and flow cytometry in AML and ALL cell lines treated with vehicle or THZ-P1-2 (1.6, 3.2, and 6.4 μM) for 24 h. Bar graphs represent the mean ± SD of at least three independent experiments and the *p* values are indicated; **p* < 0.05, ***p* < 0.01, ****p* < 0.001; ANOVA and Bonferroni post-test. **D** Alternatively, the presence of AVOs was confirmed by immunofluorescence on OCI-AML3 and NALM6 cell lines treated with vehicle or THZ-P1-2 (3.2 and 6.4 μM) for 72 h on a Lionheart FX automated microscope at magnification, ×400. The overlapping GFP and RFP channels are shown.

evidence that PIP4K2A suppresses lysosomal synthesis or enhances lysosomal turnover [16], which could explain the increase in AVOs upon treatment with THZ-P1-2 observed in this study. In brief, our data indicate that THZ-P1-2 may exert a unique pharmacological activity, acting as an inducer of the initial stages of autophagy through mitochondrial dysfunction, and as an inhibitor of the final stages of autophagy. Thus, THZ-P1-2 may leave leukemia cells in a state of "autophagic catastrophe," which reduces cell viability even in the absence of classical cell death pathways (i.e., apoptosis). Impairment of autophagy also promotes

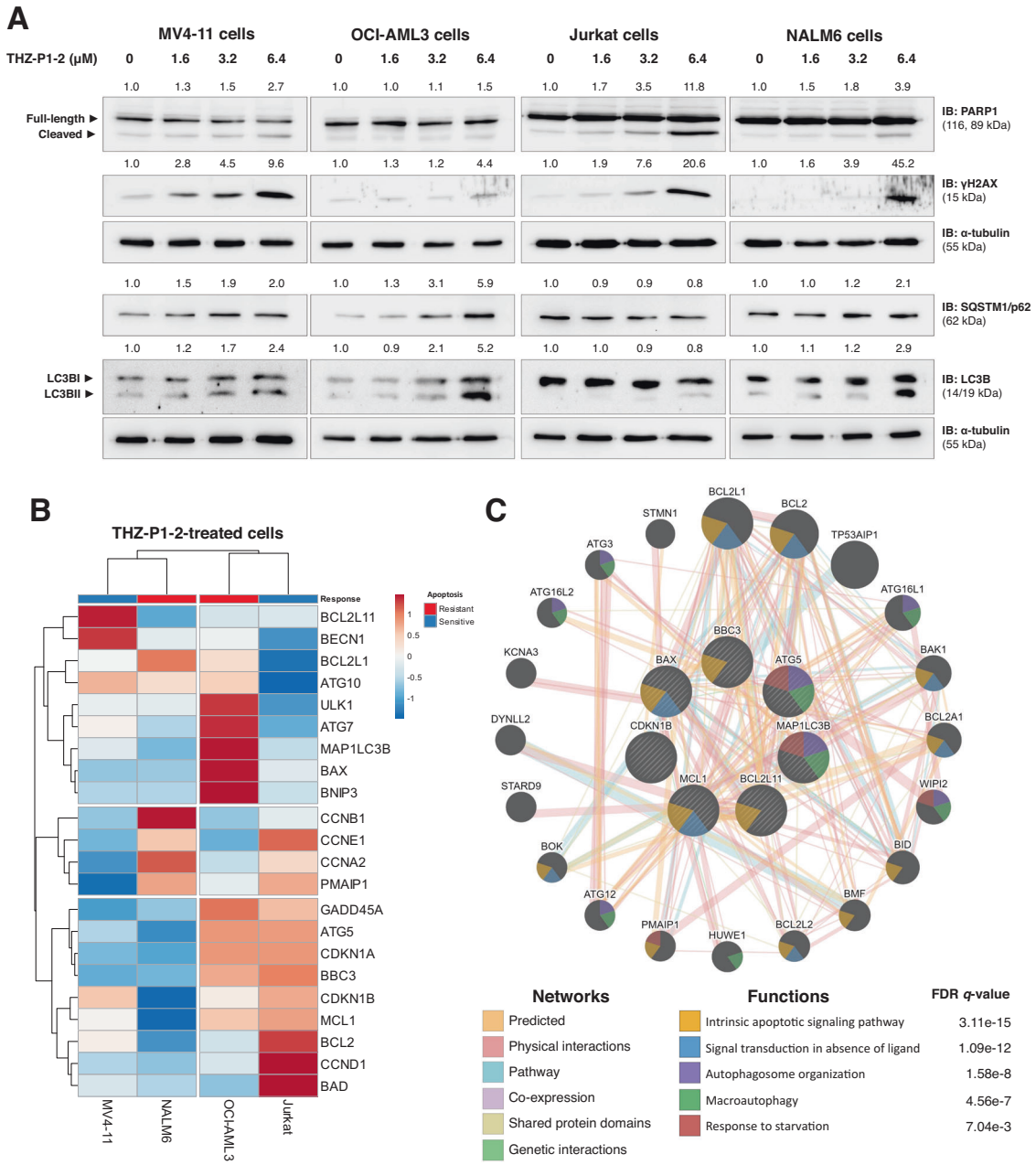

Fig. 3 THZ-P1-2 induces markers of apoptosis, DNA damage, and blockage of autophagic flow. A Western blot analysis for PARP1, γH2AX, p62/SQSTM1, and LC3B in total extracts from MV4-11, OCI-AML3, Jurkat, and NALM6 cells treated with vehicle or with increasing doses of THZ-P1-2 (1.6, 3.2, and 6.4 μM) for 24 h. Membranes were reincubated with α-tubulin antibody and developed with the SuperSignal™ West Dura Extended Duration Substrate system and GBox. Band intensities of cleaved-PARP1, γH2AX, p62/SQSTM1, and LC3B were corrected by α-tubulin expression and normalized by vehicle-treated cells. **B** Heatmap depicting the gene expression profile of leukemic cell lines treated with vehicle or THZ-P1-2 (6.4 μM) for 24 h. The blue color in the heatmap indicates decreased mRNA levels, while red indicates induced mRNA levels, which were normalized by vehicle-treated cells ($n = 4$). Leukemia cells that showed the lowest rates of THZ-P1-2-induced apoptosis were considered resistant. **C** Network for THZ-P1-2 modulated genes constructed using the GeneMANIA database (https://genemania.org/). A total of seven genes (*BBC3*, *ATG5*, *MAP1LC3B*, *MCL1*, *CDKN1B*, *BAX*, and *BCL211*) were significantly modulated in all cell lines tested and are illustrated as crosshatched circles; the interacting genes included by modeling the software are indicated by circles without crosshatched. The main biological interactions and associated functions are described in the literature.

the accumulation of mitochondrial reactive oxygen species and DNA damage [31], which was confirmed by our data.

The reduction in cellular metabolism observed upon THZ-P1-2 exposure was timely in the context of acute leukemia. Corroborating our findings, it has been demonstrated that the loss of PIP4K2s leads to alterations in mitochondrial structural and functional integrity, as observed in double PIP4K2A/B knockout mice or inhibition by shRNA in solid tumor cell lines [25]. Recent data have indicated that leukemia cells may rely more on mitochondrial metabolism and are more responsive to venetoclax [8, 32]. Since THZ-P1-2 led to mitochondrial damage and reduced cellular metabolism, we investigated the effects of the combination of both drugs on OCI-AML3 cells, a leukemia cell line that is highly resistant to venetoclax. The combined treatment showed synergistic effects, reducing the IC_{50} of venetoclax and strongly increasing apoptosis induction (Supplementary Fig. 1). Clinical

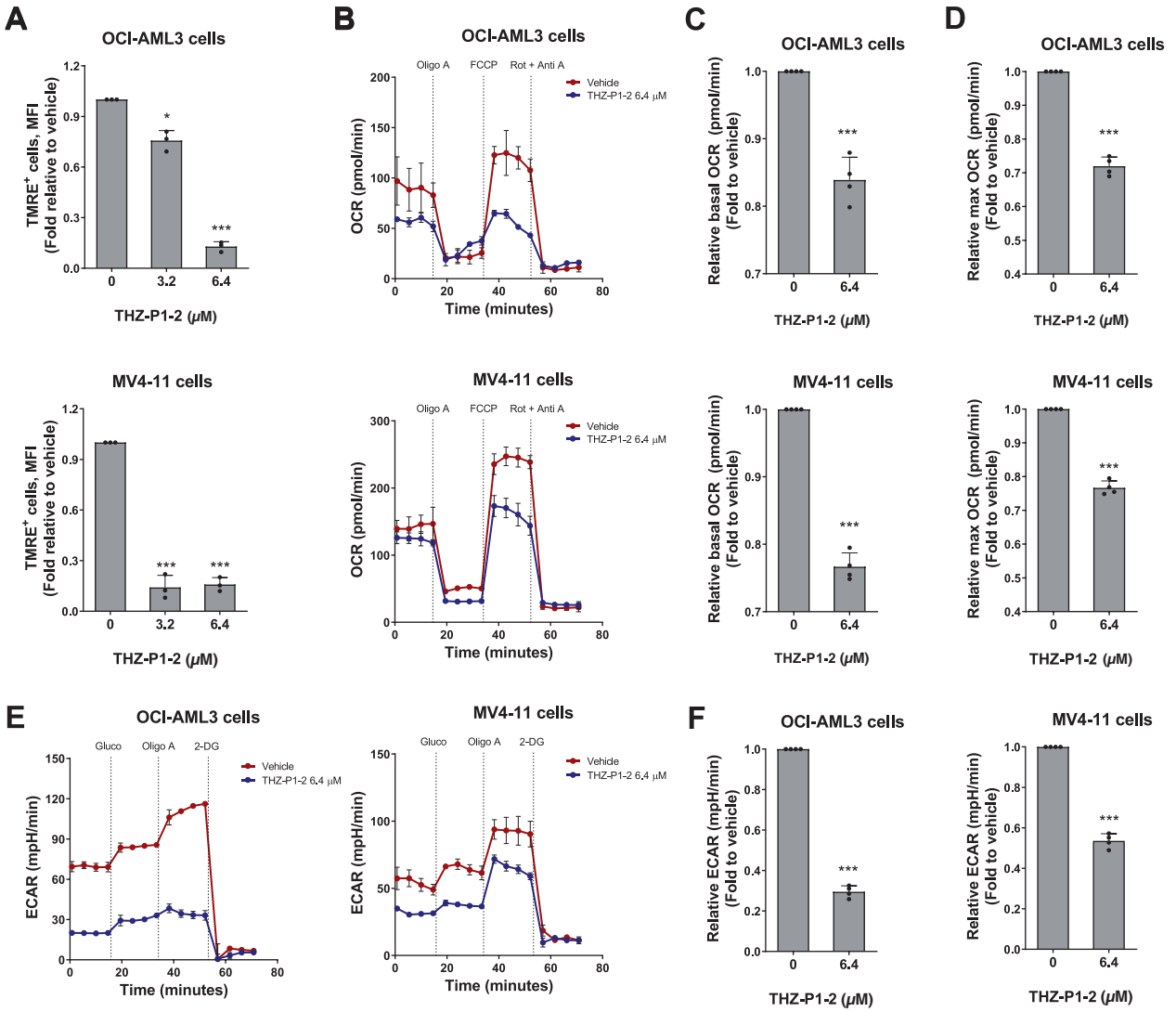

Fig. 4 THZ-P1-2 reduces cellular metabolism in leukemic cells. A Mitochondrial membrane potential analysis was evaluated using the tetramethylrhodamine, ethyl ester, perchlorate (TMRE) staining method and flow cytometry. OCI-AML3 and MV4-11 cells were treated with vehicle or THZ-P1-2 (3.2, and 6.4 μM) for 24 h. Values are expressed as the fold-change of vehicle-treated cells. Bar graphs represent the mean ± SD of at least three independent experiments and the *p* values are indicated; $*p < 0.05$, $***p < 0.0001$; ANOVA and Bonferroni post-test. **B** Oxygen consumption rate (OCR) was determined in vehicle- or THZ-P1-2-treated (6.4 μM) OCI-AML3 and MV4-11 cells using a high-resolution respirometry. A representative line graph containing OCR upon sequential addition of oligomycin (Oligo A), carbonyl cyanide-p-trifluoromethoxyphenylhydrazone (FCCP), and rotenone plus antimycin (Rot + Anti A) are illustrated; OCR was measured over time. Values are expressed as the fold-change of vehicle-treated cells. Bar graphs represent the mean ± SD of OCR at baseline (**C**) and maximum state (upon FCCP) (**D**) of at least three independent experiments. The *p* values and cell lines are indicated in the graphs; $***p < 0.0001$; Student *t*-test. **E** Extracellular acidification rate (ECAR) was evaluated in vehicle- or THZ-P1-2-treated (6.4 μM) OCI-AML3 and MV4-11 cells by Seahorse XF96 analyzer. A representative line graph containing ECAR upon sequential addition of glucose (Gluco), oligomycin (Oligo A), and 2-deoxy-D-glucose (2-DG) is illustrated; ECAR was measured over time. **F** Values are expressed as the fold-change of vehicle-treated cells. Bar graphs represent the mean ± SD of at least three independent experiments. The *p* values and cell lines are indicated in the graphs; $***p < 0.0001$; Student *t*-test.

trials with venetoclax-based regimens have shown encouraging results in hematological malignancies (i.e., AML), and the search for drug resistance markers as well as mechanisms to overcome them has been a very active field of research [33, 34]. Our preliminary findings suggest that THZ-P1-2 is a potential candidate in this context but requires further investigation. Furthermore, OXPHOS-inhibition has been associated with the disruption of stemness properties in acute leukemia [7, 35, 36], which prompted us to evaluate the effects of THZ-P1-2 on the differentiation of myeloid cells. Drug treatment upregulated the expression of differentiation markers and induced morphological changes compatible with a more differentiated phenotype (Supplementary Fig. 2). Our results are in line with a recent study suggesting that PIP4K2s are involved in the regulation of organelle crosstalk, as well as in the preservation of metabolic homeostasis [18]. The minimal effects observed in healthy CB $CD34^+$ cells suggested that THZ-P1-2 may have a favorable therapeutic window. Indeed, PIP4K2A depletion attenuated the growth of primary leukemia blasts but did not significantly affect the clonogenic or multilineage differentiation potential of healthy hematopoietic stem cells [21].

Our proteomic analysis revealed that THZ-P1-2 resistant AML $CD34^+$ (or $CD117^+$ for *NPM1*-mut AMLs) cells displayed a molecular signature similar to L-HSC and TP53 mutant AML, with a more glycolytic-driven metabolism, whereas THZ-P1-2 sensitive AML samples displayed enrichment for cell maturation markers

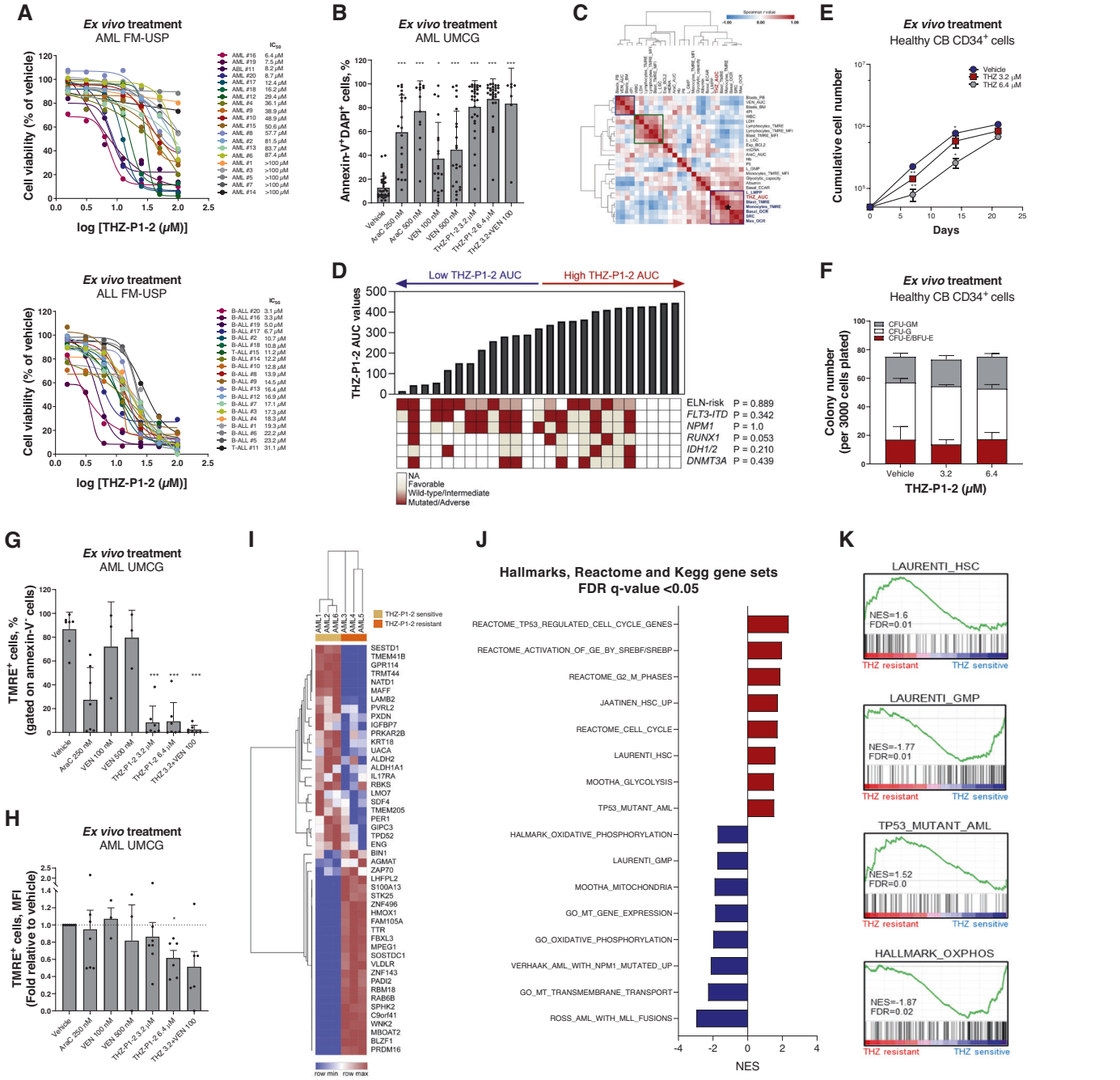

and mitochondrial metabolism, which corroborates the findings of our functional studies. The role of TP53 in the context of PIP4K2s has been recognized in several studies. In *TP53*-mutated cancer cells, the inhibition of PIP4K2A/B reduced cell survival. Similar results were observed in TP53$^{-/-}$ PIP4K2A$^{-/-}$ PIP4K2B$^{+/-}$ mice, which presented lower tumor burden and increased tumor-free survival [24]. Lundquist et al. [16] showed that *TP53* silencing enhanced the role of PIP4K2A/B inhibition in murine cell autophagy, reinforcing TP53 as an important player in response to PIP4Ks inhibition.

Our pharmacology study opens perspectives for a new class of antileukemia agents; however, it has limitations. The scope of the present study was based on in vitro and ex vivo studies, which provide relevant information to elucidate the mechanism of action and efficacy of THZ-P1-2 either alone or in combination. Considering that double knockout mice for PIP4K2A and PIP4K2B are unfeasible [24], the safety of a pan-inhibitor PIP4K2 in animal model studies should be performed. In this sense, preliminary results in leukemic animal models from other research groups indicate the antineoplastic potential of PIP4K2 inhibitors in vivo without obvious toxicity [37]. Due to the high molecular heterogeneity of our current cohort, no obvious relationship was found between any molecular disease subtype and drug response. Furthermore, the greater potency of THZ-P1-2 observed in vitro and ex vivo assays in ALL models deserves further investigation.

In conclusion, the pharmacological PIP4Ks inhibitor, THZ-P1-2 disrupts mitochondrial metabolism and autophagic flux, two cellular processes that are proposed as promising targets to improve therapeutic responses in acute leukemia. Subsequently,

Fig. 5 Pharmacological PIP4K2s inhibition selectively reduces cell viability of primary leukemic blasts. A Dose-response cytotoxicity was analyzed using a methylthiazoletetrazolium (MTT) assay in samples from acute myeloid leukemia (AML) or T- and B-acute lymphoblastic leukemia (T- or B-ALL) patients treated with vehicle or increasing concentrations of THZ-P1-2 (1.6, 3.2, 6.4, 12.5, 25, 50, and 100 μM) for 72 h. Values are expressed as the percentage of viable cells for each condition relative to vehicle-treated cells. The IC_{50} values for each patient sample are described. **B** Apoptosis was detected by flow cytometry in gated human $Sca1^{-}CD45^{+}CD34^{+}$ (or $CD117^{+}$ cells for *NPM1*-mutant AMLs) of acute myeloid leukemia (AML) samples in a co-culture system using a FITC-annexin V/DAPI staining method. Cells were treated with vehicle, cytarabine (AraC, 250 and 500 nM), venetoclax (VEN, 100 and 500 nM), and/or THZ-P1-2 (3.2 or 6.4 μM) for 72 h. Bar graphs represent the mean ± SD of all the independent patients screened, each point represents a patient. The *p* values are indicated in the graphs; $*p < 0.05$, $**p < 0.01$, $***p < 0.0001$; ANOVA and Bonferroni post-test. **C** Correlation analysis of THZ-P1-2 response with clinical, laboratory, molecular, and metabolic characteristics of the samples. Note that THZ-P1-2 responsiveness (area under curve, AUC) was clusterized with markers of mitochondrial metabolic markers (Levels of MMP in the blasts – Blast_TMRE; Basal OCR and Max OCR). Data were processed using the Morpheus platform (https://software.broadinstitute.org/morpheus/) **D** Association of THZ-P1-2 sensitivity (area under the curve, AUC), mutations in *FLT3*, *NPM1*, and *RUNX1*, and European LeukemiaNet (ELN) risk stratification. **E** Evaluation of long-term proliferation in neonatal cord blood (CB) $CD34^{+}$ and primary AML mononuclear cells using a co-culture system. Data were expressed as mean ± SD of at least three independent experiments. The time points and *p* values are indicated in the graphs; $*p < 0.05$, $**p < 0.01$, $***p < 0.0001$; ANOVA and Bonferroni post-test. **F** Neonatal cord blood (CB) $CD34^{+}$ cells were plated in cytokine-supplemented methylcellulose in the presence of vehicle or THZ-P1-2 (3.2 or 6.4 μM). Colonies were counted after 8–14 days of culture and are represented as the percent of vehicle-treated controls. Bars indicate the mean ± SD of at least three assays. **G**, **H** Mitochondrial membrane potential was detected by flow cytometry in gated human $CD45^{+}CD34^{+}$ (or $CD117^{+}$ for *NPM1*-mutant AMLs)/annexin V^{-} from samples from acute myeloid leukemia (AML) in a co-culture system using the TMRE staining method. Cells were treated with vehicle, cytarabine (AraC, 250 nM), venetoclax (VEN, 100 or 500 nM), and/or THZ-P1-2 (3.2 [alone or in combination with VEN 100 nM] or 6.4 μM) for 72 h. Bar graphs represent the mean ± SD of at least three independent experiments, each point represents a patient. The *p* values are indicated in the graphs; $*p < 0.05$, $**p < 0.01$, $***p < 0.0001$; ANOVA and Bonferroni post-test. **I** Differently expressed proteins obtained from THZ-P1-2 (THZ)-sensitive ($n = 3$) and THZ-resistant ($n = 3$) AML patients were included in the heatmap (all false discovery rate (FDR) *q* values (FDR *q*) <0.25). AML patients with higher AUC were considered resistant to THZ-P1-2. **J** The bar graph represents the normalized enrichment scores (NES) for Hallmark, Reactome, and Kegg gene sets with FDR $q < 0.05$. **K** GSEA plots for enriched molecular signatures in THZ-P1-2 (THZ) resistant *vs*. sensitive AML patient's proteome are also shown. NES and FDR *q* are indicated.

our data shed light on a new class of drugs to increase the range of treatment options for leukemia.

DATA AVAILABILITY

All the data were available from the corresponding author upon request. LFQ proteomic data were deposited under PRIDE PXD030463. The remaining data were available in the article and supplementary information. Source data are provided in this study.

REFERENCES

1. Malard F, Mohty M. Acute lymphoblastic leukaemia. Lancet. 2020;395:1146–62.
2. Short NJ, Rytting ME, Cortes JE. Acute myeloid leukaemia. Lancet. 2018;392:593–606.
3. Ley TJ, Miller C, Ding L, Raphael BJ, Mungall AJ, Robertson A, et al. Genomic and epigenomic landscapes of adult de novo acute myeloid leukemia. N Engl J Med. 2013;368:2059–74.
4. Tyner JW, Tognon CE, Bottomly D, Wilmot B, Kurtz SE, Savage SL, et al. Functional genomic landscape of acute myeloid leukaemia. Nature 2018;562:526–31.
5. Kayser S, Levis MJ. Updates on targeted therapies for acute myeloid leukaemia. Br J Haematol. 2022;196:316–28.
6. Rashkovan M, Ferrando A. Metabolic dependencies and vulnerabilities in leukemia. Genes Dev. 2019;33:1460–74.
7. de Beauchamp L, Himonas E, Helgason GV. Mitochondrial metabolism as a potential therapeutic target in myeloid leukaemia. Leukemia. 2022;36:1–12.
8. Lagadinou ED, Sach A, Callahan K, Rossi RM, Neering SJ, Minhajuddin M, et al. BCL-2 inhibition targets oxidative phosphorylation and selectively eradicates quiescent human leukemia stem cells. Cell Stem Cell. 2013;12:329–41.
9. Jones CL, Stevens BM, D'Alessandro A, Reisz JA, Culp-Hill R, Nemkov T, et al. Inhibition of amino acid metabolism selectively targets human leukemia stem cells. Cancer Cell. 2018;34:724–40.e724.
10. Pollyea DA, Stevens BM, Jones CL, Winters A, Pei S, Minhajuddin M, et al. Venetoclax with azacitidine disrupts energy metabolism and targets leukemia stem cells in patients with acute myeloid leukemia. Nat Med. 2018;24:1859–66.
11. Rafiq S, McKenna SL, Muller S, Tschan MP, Humbert M. Lysosomes in acute myeloid leukemia: potential therapeutic targets? Leukemia. 2021;35:2759–70.
12. Sehgal AR, Konig H, Johnson DE, Tang D, Amaravadi RK, Boyiadzis M, et al. You eat what you are: autophagy inhibition as a therapeutic strategy in leukemia. Leukemia. 2015;29:517–25.
13. Arora GK, Palamiuc L, Emerling BM. Expanding role of PI5P4Ks in cancer: a promising druggable target. FEBS Lett. 2022;596:3–16.
14. Tan X, Thapa N, Choi S, Anderson RA. Emerging roles of PtdIns(4,5)P2-beyond the plasma membrane. J Cell Sci. 2015;128:4047–56.
15. Vicinanza M, Korolchuk VI, Ashkenazi A, Puri C, Menzies FM, Clarke JH, et al. PI(5)P regulates autophagosome biogenesis. Mol Cell. 2015;57:219–34.
16. Lundquist MR, Goncalves MD, Loughran RM, Possik E, Vijayaraghavan T, Yang A, et al. Phosphatidylinositol-5-phosphate 4-kinases regulate cellular lipid metabolism by facilitating autophagy. Mol Cell. 2018;70:531–44.
17. Hu A, Zhao XT, Tu H, Xiao T, Fu T, Wang Y, et al. PIP4K2A regulates intracellular cholesterol transport through modulating PI(4,5)P2 homeostasis. J Lipid Res. 2018;59:507–14.
18. Ravi A, Palamiuc L, Emerling BM. Crucial players for inter-organelle communication: PI5P4Ks and their lipid product PI-4,5-P2 come to the surface. Front Cell Dev Biol. 2021;9:791758.
19. Xu H, Yang W, Perez-Andreu V, Devidas M, Fan Y, Cheng C, et al. Novel susceptibility variants at 10p12.31-12.2 for childhood acute lymphoblastic leukemia in ethnically diverse populations. J Natl Cancer Inst. 2013;105:733–42.
20. Walsh KM, de Smith AJ, Chokkalingam AP, Metayer C, Dahl GV, Hsu LI, et al. Novel childhood ALL susceptibility locus BMI1-PIP4K2A is specifically associated with the hyperdiploid subtype. Blood. 2013;121:4808–9.
21. Jude JG, Spencer GJ, Huang X, Somerville TDD, Jones DR, Divecha N, et al. A targeted knockdown screen of genes coding for phosphoinositide modulators identifies PIP4K2A as required for acute myeloid leukemia cell proliferation and survival. Oncogene. 2015;34:1253–62.
22. Zhang S, Li Z, Yan X, Bao L, Deng Y, Zeng F, et al. Regulatory network and prognostic effect investigation of PIP4K2A in leukemia and solid cancers. Front Genet. 2018;9:721.
23. Lima K, Coelho-Silva JL, Kinker GS, Pereira-Martins DA, Traina F, Fernandes P, et al. PIP4K2A and PIP4K2C transcript levels are associated with cytogenetic risk and survival outcomes in acute myeloid leukemia. Cancer Genet. 2019;233-234:56–66.
24. Emerling BM, Hurov JB, Poulogiannis G, Tsukazawa KS, Choo-Wing R, Wulf GM, et al. Depletion of a putatively druggable class of phosphatidylinositol kinases inhibits growth of p53-null tumors. Cell 2013;155:844–57.
25. Ravi A, Palamiuc L, Loughran RM, Triscott J, Arora GK, Kumar A, et al. PI5P4Ks drive metabolic homeostasis through peroxisome-mitochondria interplay. Dev Cell. 2021;56:1661–76.
26. Sivakumaren SC, Shim H, Zhang T, Ferguson FM, Lundquist MR, Browne CM, et al. Targeting the PI5P4K lipid kinase family in cancer using covalent inhibitors. Cell Chem Biol. 2020;27:525–37.e526.
27. Thome MP, Filippi-Chiela EC, Villodre ES, Migliavaca CB, Onzi GR, Felipe KB, et al. Ratiometric analysis of Acridine Orange staining in the study of acidic organelles and autophagy. J Cell Sci. 2016;129:4622–32.
28. Livak KJ, Schmittgen TD. Analysis of relative gene expression data using real-time quantitative PCR and the 2(-delta delta C(T)) method. Methods. 2001;25:402–8.
29. de Boer B, Prick J, Pruis MG, Keane P, Imperato MR, Jaques J, et al. Prospective isolation and characterization of genetically and functionally distinct AML subclones. Cancer Cell. 2018;34:674–89.e678.

30. Subramanian A, Tamayo P, Mootha VK, Mukherjee S, Ebert BL, Gillette MA, et al. Gene set enrichment analysis: a knowledge-based approach for interpreting genome-wide expression profiles. Proc Natl Acad Sci USA. 2005;102:15545–50.
31. Auberger P, Puissant A. Autophagy, a key mechanism of oncogenesis and resistance in leukemia. Blood. 2017;129:547–52.
32. Chen X, Glytsou C, Zhou H, Narang S, Reyna DE, Lopez A, et al. Targeting mitochondrial structure sensitizes acute myeloid leukemia to venetoclax treatment. Cancer Disco. 2019;9:890–909.
33. Foran JM. Can venetoclax-based therapy replace 7+3 induction in fit older adults with AML? Best Pr Res Clin Haematol. 2021;34:101335.
34. Xu Y, Ye H. Progress in understanding the mechanisms of resistance to BCL-2 inhibitors. Exp Hematol Oncol. 2022;11:31.
35. Egan G, Khan DH, Lee JB, Mirali S, Zhang L, Schimmer AD. Mitochondrial and metabolic pathways regulate nuclear gene expression to control differentiation, stem cell function, and immune response in leukemia. Cancer Disco. 2021;11:1052–66.
36. Kuntz EM, Baquero P, Michie AM, Dunn K, Tardito S, Holyoake TL, et al. Targeting mitochondrial oxidative phosphorylation eradicates therapy-resistant chronic myeloid leukemia stem cells. Nat Med. 2017;23:1234–40.
37. McElligott DL, Kesicki E, Karukarichi K, Shim H, Wang R, Yu AS, et al. Development of inhibitors of PIP4K2 as a treatment for patients with hematologic malignancies. Blood. 2018;132:213.

ACKNOWLEDGEMENTS

KL received a fellowship from FAPESP (grant #2020/12842-0). IW received a fellowship from FAPESP (grant #2015/09228-0). DAP-M received a fellowship from FAPESP (grant #2017/23117-1). IW and DAP-M were sponsored by the Abel Tasman Talent Program (ATTP) of the Graduate School of Medical Sciences of the University of Groningen/University Medical Center Groningen (UG/UMCG), Netherlands. This study was supported by grants #2019/23864-7 and #2021/11606-3 from the São Paulo Research Foundation (FAPESP). This study was financed in part by the Coordenação de Aperfeiçoamento de Pessoal de Nível Superior, Brasil (CAPES), Finance Code 001. The authors thank Prof. Carlos Frederico Martins Menck for assistance with the comet assay and critical review of the manuscript.

AUTHOR CONTRIBUTIONS

Conceptualization: KL, EMR, and JAM-N; investigation: KL, DAP-M, LBLM, IW, JJS, EG, EMR, and JAM-N; technical assistance and discussion: JLC-S, GSL, RCC, AML, WFSJ, APAdLL, EDRPV, JRH, and GH; resources: GH; data curation: KL, DAP-M, JJS, EMR, JAM-N; writing—original draft: KL, DAP-M, JJS, EMR, and JAM-N; writing—review and editing: LBLM, JLC-S, GSL, IW, RCC, AML, WFSJ, APAdLL, EDRPV, EG, JRH, and GH; funding acquisition: JJS, EMR, and JAM-N; overall supervision: EMR, and JJS.

COMPETING INTERESTS

The authors declare no competing interests.

ADDITIONAL INFORMATION

Supplementary information The online version contains supplementary material available at https://doi.org/10.1038/s41408-022-00747-w.

Correspondence and requests for materials should be addressed to Eduardo Magalhães Rego or João Agostinho Machado-Neto.

Reprints and permission information is available at http://www.nature.com/reprints

Publisher's note Springer Nature remains neutral with regard to jurisdictional claims in published maps and institutional affiliations.